Analyzing powers of polarized deuterons in low-energy ^{6}Li$(d, \alpha)^4$He and ^{6}Li$(d, p_0)^7$Li reactions in a resonance region

M. Yamaguchi* and Y. Tagishi
The Institute of Physical and Chemical Research (RIKEN), 2-1 Hirosawa, Wako, Saitama 351-0198, Japan

Y. Aoki, T. Iizuka, T. Nagatomo, T. Shinba, N. Yoshimaru, and Y. Yamato
Institute of Physics and Tandem Accelerator Center, University of Tsukuba, Tsukuba, Ibaraki 305-8577, Japan

T. Katabuchi
Gunma University Graduate School of Medicine, Maebashi, Gunma 371-8511, Japan

M. Tanifuji
Department of Physics, Hosei University, Tokyo 102-8160, Japan
(Received 1 December 2005; revised manuscript received 5 August 2006; published 12 December 2006)

Low-energy ^{6}Li$(d, \alpha)^4$He and ^{6}Li$(d, p_0)^7$Li reactions are affected by the 2^+ resonance level of ^{8}Be at $E_x \simeq 22.2$ MeV. In this work, we present a new method to extract fractions of the 2^+ components of the reactions, which include the resonance, by using the tensor-analyzing powers, T_{2q}, of polarized deuterons. We measured T_{2q} for $q = 0, 1, 2$ at the very low incident energy $E_d = 90$ keV and analyzed the data by the invariant amplitude method giving the 2^+ fractions as 0.90 ± 0.05 for ^{6}Li(d, p) and 0.998 ± 0.003 for ^{6}Li(d, α). For ^{6}Li(d, p), it was comparable to the resonance fraction extracted from cross-section data, whereas for ^{6}Li(d, α), the 2^+ fraction was much larger than the resonance fraction extracted from cross-section data. A part of the analyses was extended to higher energies up to 960 keV.

DOI: 10.1103/PhysRevC.74.064606 PACS number(s): 21.10.Jx, 24.10.−i, 24.70.+s, 25.45.Hi

I. INTRODUCTION

Nuclear reactions at extremely low energies are an important subject in astrophysics as the mechanism of producing elements in the universe. Generally, cross sections of the reactions between charged particles decrease exponentially when the incident energy decreases because of the Coulomb barrier. Then, in the astrophysics, the $S(E)$ factor,

$$S(E) = \sigma(E) E \exp(2\pi\eta),$$

is used to express the strength of the reaction, where σ is the cross section, E is the reaction energy in the center-of-mass (c.m.) system, and η is the Sommerfeld parameter. When cross-section data are not available at a given energy, for example, due to the smallness of the cross section, one should extrapolate the astrophysical $S(E)$ factor from data in a higher-energy region. However, because the extrapolation process requires an appropriate reaction model, the choice of the model is an important factor in the extraction, because the obtained $S(E)$ factor may depend on the reaction model [1,2].

Such model-dependent analyses are applied when the cross section has resonance components as well as nonresonance ones. In this case, the resonant-component fraction is particularly important for the extrapolation process of $S(E)$. However, the extraction of the resonance component from the cross-section data suffers from inevitable difficulties at low energies. As discussed above, the absolute magnitude of the cross section decreases with a decrease of the incident energy, resulting in difficulties concerning the measurement. Furthermore, the angular distribution of the cross section has a tendency to become isotropic at low energies because of the dominance of the s-wave in the incident channel. However, separation of the cross section into the resonance and nonresonance components essentially utilizes the anisotropy of the angular distribution. Therefore, in the low-energy region, the cross section will not be the favorite observable for extracting of the resonance component and one will need supplements by different approaches with other observables. As one of such approaches, we present a method that uses polarization observables to extract the fraction of a particular spin-parity state, at very low energies. When the resonance configuration is exclusively dominant in the state, it will provide the resonance fraction.

We measured the vector- and tensor-analyzing powers of polarized deuterons at the incident energy of 90 keV in the ^{6}Li$(d, p_0)^7$Li (g.s.) and ^{6}Li$(d, \alpha)^4$He (g.s.) reactions and analyzed the data by using the invariant amplitude method [3], which allowed model-independent analyses of reactions. Low incident energies, such as the present one, have advantages for applying the method. At low energies, the penetrability of the centrifugal barrier restricts the orbital angular momentum of the incident beam to a few values near to the s-wave, and thus the reaction can be described by the invariant amplitudes of small number, which are treated as angle-independent constants. Further, because the resonance level is located in the energy close to the threshold of the $d + ^6$ Li channel, such

*Electronic address: myamagu@rarfaxp.riken.jp

a low incident energy will be advantageous for investigating details of the resonance effects.

The present calculation well reproduced the measured analyzing powers. Through the analysis of the data, we confirmed the spin-parity of the resonance to be 2^+ and obtained the fraction of the 2^+ configuration, which includes the resonance, for the (d, p_0) reaction as 0.9±0.05, which is comparable to the compound-nucleus fraction, about 0.85 [4], extracted from the cross-section data. For the (d, α) reaction, we obtained 0.998±0.003 for the 2^+ fraction, which is much larger than the compound-nucleus fraction, about 0.5, estimated from the S factor in Ref. [2], where the cross sections were employed in the analysis. Moreover, the present analyses gave a deeper understanding of the reactions than earlier ones. For example, at higher energies, 600 and 960 keV, the analyzing powers for the (d, p) reaction on the ^{6}Li target had been measured by M. Glor *et al.* [5] and analyzed by the R-matrix theory. They found that the dominant component of the reaction is due to the 2^+ state but had not derived the fraction of the component. Further the nature of the differences between the measured analyzing powers and the contributions of the 2^+ state had not been clarified. At $E_d = 90$ keV, we explained the differences as dominantly being contributions of the nonresonant s wave via the 1^+ state of the $d + {}^6$Li system and those of p waves. A part of such analyses were extended to higher energies up to 960 keV in both of the (d, p) and (d, α) reactions.

II. EXPERIMENTAL SETUP AND RESULT

The experiment was performed using a Lamb shift-type polarization ion source [6] at the University of Tsukuba Tandem Accelerator Center (UTTAC). The polarization of the deuteron beam was measured by the quench-ratio method [7] about every 2 h. The typical value of the beam intensity was about 100 nA, and that of the beam polarization was about 0.70. The uncertainty of the polarization was about 0.02.

Figure 1 shows the placement of the detectors and the target. The target was a layer of lithium carbonate, Li_2CO_3, having a thickness of about 10 μg/cm^2 on an aluminum backing having a thickness of about 15 μm. The enrichment of ^{6}Li was 95%.

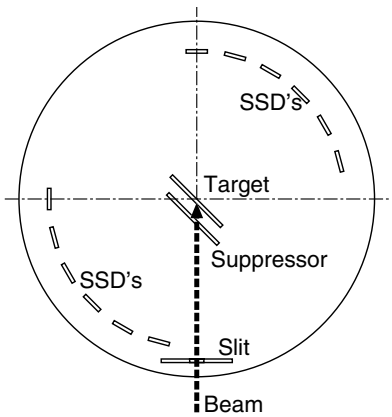

FIG. 1. Layout in the scattering chamber.

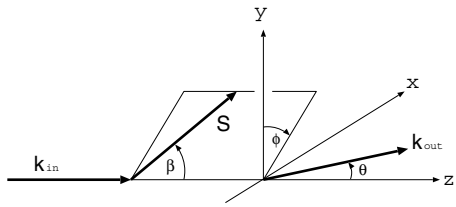

FIG. 2. Coordinate system in which the polarization state of the incident beam is described. The z axis is along the momentum of the incident particle, $\boldsymbol{k}_{\rm in}$. The y axis is along $\boldsymbol{k}_{\rm in} \times \boldsymbol{k}_{\rm out}$, where $\boldsymbol{k}_{\rm out}$ represents the outgoing momentum direction. The spin orientation $\boldsymbol{S}$ makes the angle β with respect to $\boldsymbol{k}_{\rm in}$. The projection of $\boldsymbol{S}$ onto the xy plane makes the angle ϕ with respect to the y axis.

The beam was introduced to the lithium carbonate layer and was intercepted by the aluminum backing, which played the role of a Faraday cup. A slit with a diameter of 5 mm was placed at a distance of 150 mm upstream from the target. The energy loss in the layer of lithium carbonate was about 8 keV. A meshed sheet of SUS supplied with a voltage of −300 V was placed in front of the target to suppress the secondary emission electrons from the target. We placed 12 Si-SSDs around the target at every 15° scattering angles from 0° to 165°. Each detector was placed at a distance of 140 mm from the target and had a solid angle of 10 msr. On each Si-SSD placed in the range of scattering angles from 90° to 165°, a mylar sheet having a thickness of 9 μm was placed to block elastic deuterons.

The polarizations of the incident particle were set up in the following manner. The reference frame was chosen as in Figure 2, which is similar to that in Ref. [8]. The z axis is along the momentum of the incident particle $\boldsymbol{k}_{\rm in}$. The y axis is along $\boldsymbol{k}_{\rm in} \times \boldsymbol{k}_{\rm out}$, where $\boldsymbol{k}_{\rm out}$ represents the momentum of the outgoing particle. The spin orientation $\boldsymbol{S}$ makes the angle β with respect to $\boldsymbol{k}_{\rm in}$. The projection of $\boldsymbol{S}$ onto the xy plane makes the angle ϕ with respect to the y axis. For measurements of iT_{11} and A_{yy}, the spin orientation $\boldsymbol{S}$ was chosen along the y axis ($\beta = 90°$, $\phi = 0°$). For this choice of the spin orientation,

$$iT_{11} = \frac{1}{2\sqrt{3}N_{\rm u}}\left[\left(\frac{N_1}{P_1} - \frac{N_{-1}}{P_{-1}}\right) - \left(\frac{N_{\rm u}}{P_1} - \frac{N_u}{P_{-1}}\right)\right], \quad (1)$$

and

$$A_{yy} = \frac{1}{P_0}\left(1 - \frac{N_0}{N_{\rm u}}\right) \quad (2)$$

with

$$N_{\rm u} = \left(\frac{N_1}{P_1} + \frac{N_0}{P_0} + \frac{N_{-1}}{P_{-1}}\right) \Big/ \left(\frac{1}{P_1} + \frac{1}{P_0} + \frac{1}{P_{-1}}\right), \quad (3)$$

where N_m and P_m ($m = 1, 0,$ or -1) are the yield and the polarization for the spin magnetic substate m. The beam from lamb shift-type polarization ion source consists of an unpolarized component and a perfectly polarized one. The beam polarization P_m is described as the fraction of the polarized one. In the case of our ion source, P_m follows the relation,

$$P_1 = \frac{P_0}{0.963} = \frac{P_{-1}}{0.931}. \quad (4)$$

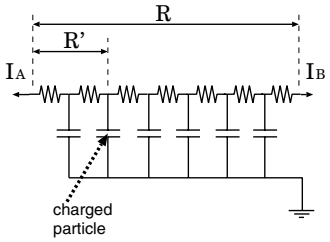

FIG. 3. Circuit including the Si-SSD. Each Si-SSD is written as a condenser.

For the measurements of T_{20}, the spin orientation was chosen along $\boldsymbol{k}_{\rm in}$ ($\beta = 0^\circ$). We obtained

$$T_{20} = \frac{\sqrt{2}(N_1 - N_0)}{P_1 N_0 + 2P_0 N_1}. \tag{5}$$

and

$$T_{22} = -\frac{A_{yy}}{\sqrt{3}} - \frac{T_{20}}{\sqrt{6}}. \tag{6}$$

For the measurement of T_{21}, β was chosen to be 54.7°, which satisfies $3\cos^2\beta = 1$, and ϕ was chosen as 90°. Then T_{21} was described as

$$T_{21} = \frac{1}{\sqrt{3}P_1 \sin(2 \times 54.7^\circ)} \left(\frac{2N_1 - N_0}{2P_0 N_1 + P_1 N_0} - \frac{2}{\sqrt{3}} P_1 T_{22} \right). \tag{7}$$

Figure 3 shows the circuit, including the detectors. Each Si-SSD is written as a condenser. Each coadjacent pair of detectors is divided by a resister. The energy of the detected particle is proportional to the sum of two currents, $I_{\rm A}$ and $I_{\rm B}$. The active detector is identified by using a signal that is proportional to the value $P = I_{\rm A}/(I_{\rm A} + I_{\rm B})$. P is represented as

$$P = 1 - \frac{R'}{R},$$

where R is the total resistance of the circuit, R' is the resistance of the left side from the active detector.

Figure 4 shows the spectrum measured by a detector. The measured analyzing powers for the ^{6}Li(d, p) and ^{6}Li(d, α) reactions are given in Tables I and II, respectively, and graphed in Fig. 5. The data show remarkable characteristics.

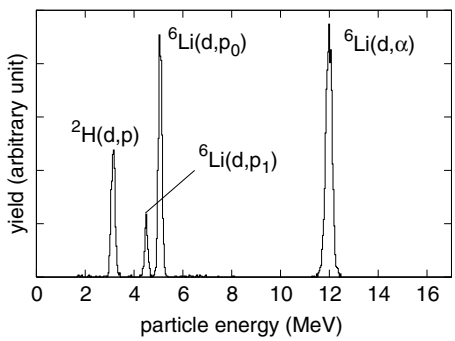

FIG. 4. Spectrum measured by a detector.

In the (d, p) reaction, the angular distributions of the vector- and tensor-analyzing powers are approximately described by $\sin\theta$ and the Legendre function $P_{2q}(\cos\theta)$, respectively, except for sign and magnitude. In the (d, α) reaction, the latter analyzing powers,which are shown up to $\theta = 90^\circ$, have angular distributions similar to those in the (d, p) reaction but with the opposite sign, whereas the former one is almost zero. These characteristics of the analyzing powers are explained by the invariant amplitude method, which is described in the next section.

The anisotropy of the cross section of ^{6}Li(d, p_0) reaction, which is considered to be the initial p-wave effect, was estimated by using the same data set. The yield for unpolarized beam was obtained by recomposing the yields for polarized beams. The cross section is described by referring to that of the (d, α) reaction. The latter angular distribution is expected to be isotropic, because contributions of the incident p wave are canceled due to the identical two bosons in the final states and those of higher partial waves are negligibly small as discussed in Sec. III B. Then the quotient of the yield for ^{6}Li(d, p_0) divided by that for ^{6}Li(d, α) represents the anisotropy of the ^{6}Li(d, p_0) cross section and is given in Table III and displayed in Fig. 6. In the figure, most of the data points of the quotient are described by the angular distribution, $0.576(1 + 2 \times 0.008\cos\theta)$, when the experimental errors are taken into account, although a few data points deviates from the line. In the next section, it is examined if details of the angular distribution bring about ambiguities in analysis of the analyzing powers.

III. ANALYSIS

We analyzed the data by the invariant amplitude method [3], the essence of which is briefly summarized below. Additional approximations applicable to low-energy reactions, were introduced as discussed in Sec. I. That is, the available incident partial wave is restricted to s, p, and d waves and the angular dependence of the invariant amplitude is neglected [9]. In the invariant amplitude method, transition amplitudes are decomposed into spin-space tensors, designated by the rank, K, which describes the spin-space nature of the concerned interactions; for example, when the parity of the system is not changed, scalar amplitudes ($K = 0$) denote scattering by central interactions, vector ones ($K = 1$) that by the spin vector interactions like LS ones, and so on. With these amplitudes, the physical observables are similarly decomposed and the components are classified according to the tensor rank involved.

The analyzing powers, T_{kq}, of a polarized beam for the reaction $\vec{a} + A \to b + B$ is described by the use of the T matrix $\boldsymbol{M}$ as

$$T_{kq} = \frac{1}{N_R} \mathrm{Tr}(\boldsymbol{M}\tau_{kq}\boldsymbol{M}^\dagger), \tag{8}$$

where $N_R = \mathrm{Tr}(\boldsymbol{M}\boldsymbol{M}^\dagger)$ and τ_{kq} is the spin-tensor operator of the particle a with the rank k and the z component q [8]. In the present theoretical frame, T_{kq} is given by

$$T_{kq} = \sum_{K K'} T_{kq}(K, K'). \tag{9}$$

TABLE I. Measured analyzing powers for the ^{6}Li(d, p) reaction. The errors are statistical.

$\theta_{\mathrm{c.m.}}$(deg.)	iT_{11}	T_{20}	T_{21}	T_{22}
0.0	0.007 ± 0.014	0.418 ± 0.016	-0.007 ± 0.030	0.008 ± 0.031
15.4	-0.009 ± 0.013	0.401 ± 0.017	-0.111 ± 0.028	0.024 ± 0.028
30.7	-0.073 ± 0.014	0.322 ± 0.017	-0.218 ± 0.030	0.055 ± 0.030
46.0	-0.088 ± 0.012	0.176 ± 0.018	-0.291 ± 0.027	0.116 ± 0.027
61.3	-0.110 ± 0.013	0.083 ± 0.017	-0.249 ± 0.028	0.178 ± 0.029
76.4	-0.114 ± 0.011	-0.098 ± 0.018	-0.183 ± 0.025	0.233 ± 0.026
91.5	-0.123 ± 0.013	-0.159 ± 0.018	-0.086 ± 0.027	0.277 ± 0.029
106.4	-0.106 ± 0.011	-0.119 ± 0.018	0.063 ± 0.023	0.312 ± 0.026
121.3	-0.071 ± 0.019	-0.093 ± 0.023	0.170 ± 0.036	0.198 ± 0.039
136.0		0.041 ± 0.034		
150.7	-0.022 ± 0.020	0.200 ± 0.021	0.201 ± 0.036	0.055 ± 0.041
165.4		0.338 ± 0.028		

For the vector and tensor analyzing powers, iT_{11} and T_{2q},

$$iT_{11}(K, K') = \frac{1}{N_R} \sum_{l_i, l_i'} Y_{l_i l_i'}(K, K') \times Q_{11, l_i l_i'}(K, K'), \quad (10)$$

$$T_{2q}(K, K') = \frac{1}{N_R} \sum_{l_i, l_i'} X_{l_i l_i'}(K, K') \times Q_{2q, l_i l_i'}(K, K'), \quad (11)$$

where N_R is proportional to differential cross sections and is given by

$$N_R = \sum_K N_R(K, K), \quad (12)$$

$$N_R(K, K) = \sum_{l_i = \overline{K} - K}^{K} \sum_{l_i' = \overline{K}' - K'}^{K'} \times Q_{00, l_i l_i'}(K, K) Z_{l_i l_i'}(K, K), \quad (13)$$

with

$$X_{l_i l_i'}(K, K') = \sum_{s_i s_i' s_f} \hat{s}_i \hat{s}_i' \hat{s}_\mathrm{a} W(s_i' s_\mathrm{a} 2 s_\mathrm{a}; s_\mathrm{a} s_i) \times W(2 s_i K' s_f; s_i' K) \times \mathrm{Re}\{F^*(s_i s_f K l_i) F(s_i' s_f K' l_i')\}, \quad (14)$$

$$Y_{l_i l_i'}(K, K') = \sum_{s_i s_i' s_f} \hat{s}_i \hat{s}_i' \hat{s}_\mathrm{a} W(s_i' s_\mathrm{a} 1 s_\mathrm{a}; s_\mathrm{a} s_i) \times W(1 s_i K' s_f; s_i' K) \times \mathrm{Im}\{F^*(s_i s_f K l_i) F(s_i' s_f K' l_i')\}, \quad (15)$$

$$Z_{l_i l_i'}(K, K) = \sum_{s_i s_f} \mathrm{Re}\{F^*(s_i s_f K l_i) F(s_i s_f K l_i')\}. \quad (16)$$

Here, s_a denotes the spin of the particle a, $s_i(s_f)$ the initial (final) channel spin and l_i the incident orbital angular momentum. The function F is the invariant amplitude and Q is a function of $\cos\theta$ and $\sin\theta$. Their explicit forms are given in Tables I–V in Ref. [3] for $K, K' \leqslant 2$.

We apply the above formulas to the reactions ^{6}Li$(d, p)^7$Li(g.s.) and ^{6}Li$(d, \alpha)^4$He. The $d + ^6$Li system at the present energy is situated under a broad resonance that had been described as a 2^+ resonance with the 800-keV width located at 80 keV below the reaction threshold [10,11]. Also some isospin mixing effects had been reported for the state [4]. Furthermore, the recent analysis of related reactions by the R-matrix theory [12] predicted that this broad resonance consists of two components of the same spin parity, 2^+; one located at $E_x = 22.09$ MeV with $\Gamma = 580$ keV and the other at $E_x = 22.78$ keV with $\Gamma = 1670$ keV. However, the present incident energy is covered by both of these components, and it is difficult to discriminate apriori their contributions one from other. Then we treat them as a whole by describing as the 2^+ contribution, which accordingly includes all contributions of the 2^+ configurations at the given energy.

TABLE II. Measured analyzing powers for the ^{6}Li(d, α) reaction. The errors are statistical.

$\theta_{\mathrm{c.m.}}$(deg.)	iT_{11}	T_{20}	T_{21}	T_{22}
0.0	-0.018 ± 0.021	-0.578 ± 0.039	0.005 ± 0.014	0.031 ± 0.054
10.3	-0.017 ± 0.021	-0.551 ± 0.039	0.132 ± 0.016	0.011 ± 0.053
30.9	-0.013 ± 0.021	-0.405 ± 0.037	0.330 ± 0.020	-0.097 ± 0.044
51.4	0.014 ± 0.021	-0.089 ± 0.034	0.369 ± 0.023	-0.270 ± 0.030
71.7	-0.003 ± 0.021	0.146 ± 0.031	0.244 ± 0.023	-0.389 ± 0.033
91.8	0.004 ± 0.021	0.253 ± 0.030	-0.008 ± 0.021	-0.394 ± 0.036

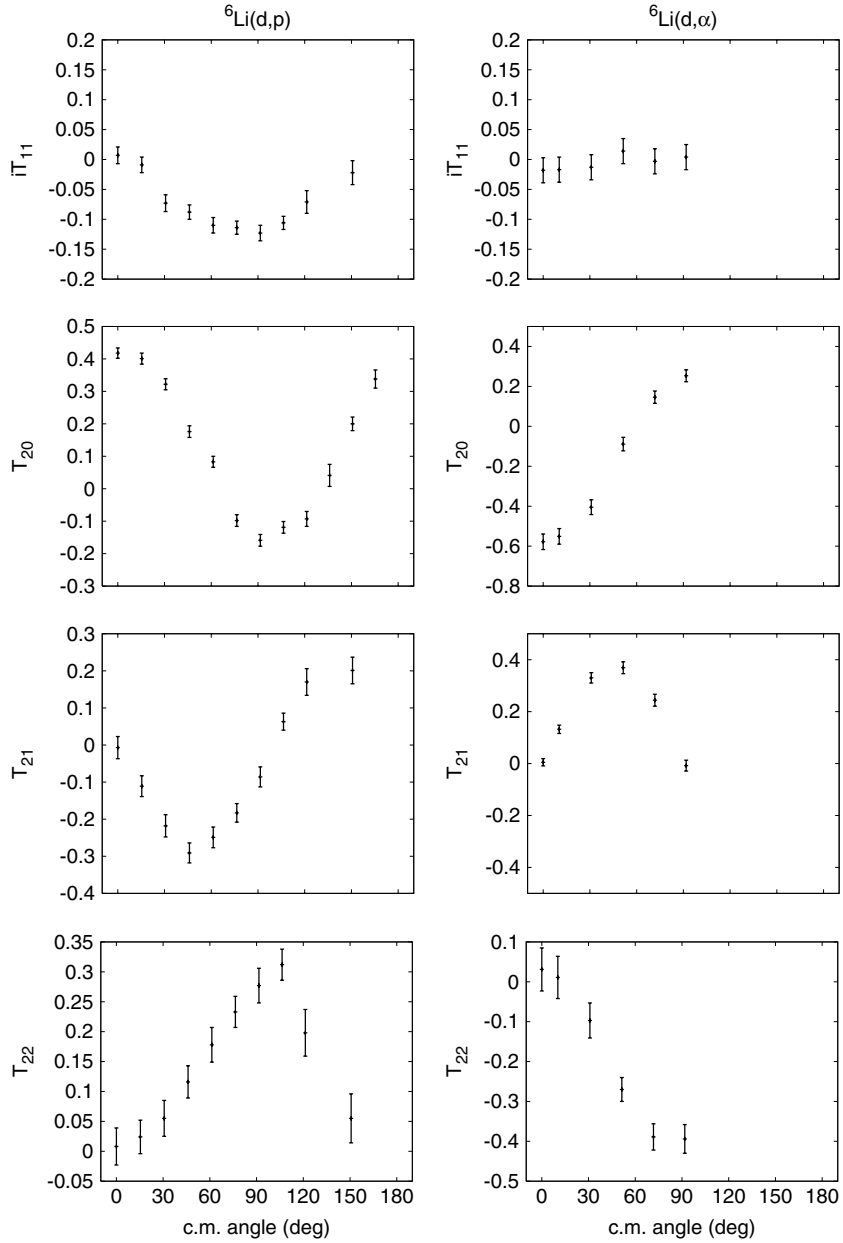

FIG. 5. Experimental results for ^{6}Li(d, p)^{7}Li (left column) and ^{6}Li(d, α)^{4}He (right column). The abscissas represent the scattering angle in the c.m. system.

TABLE III. Quotient of the yield of ^{6}Li(d, p_0) divided by the yield of ^{6}Li(d, α).

$\theta_{\text{c.m.}}$(deg.)	Quotient
0.0	0.588 ± 0.012
5.4	0.587 ± 0.011
30.7	0.587 ± 0.012
46.0	0.597 ± 0.011
61.3	0.585 ± 0.011
76.4	0.565 ± 0.010
91.5	0.556 ± 0.008
106.4	0.583 ± 0.008
121.3	0.567 ± 0.013
136.0	0.599 ± 0.013
150.7	0.557 ± 0.013
165.4	0.569 ± 0.012

A. ^{6}Li(d, p_0)

First, we analyzed the ^{6}Li(d, p_0) reaction. In this case $s_A = s_a = 1$ and $s_B = \frac{3}{2}$, $s_b = \frac{1}{2}$. Then, the initial channel spin was $s_i = 0, 1, 2$ and the final one was $s_f = 1, 2$. Because $\boldsymbol{s}_i + \boldsymbol{K} = \boldsymbol{s}_f$, $K = 0, 1, 2, 3, 4$. In the present reaction, the parity of the system is changed by the reaction from positive to negative ($\Delta P \neq 0$), and then the amplitudes of $K = 0$ vanish. The amplitudes induced by central forces appear as an amplitude of $K = 1$, because the p-state wave function of the captured neutron in the final nucleus transforms the original amplitudes by multiplying a vector. Similarly, the amplitudes by LS interactions appear as those of $K = 0, 1, 2$, and the amplitudes by tensor interactions as $K = 1, 2, 3$. In the following, contributions of $K = 3$ amplitudes will be neglected because they are induced by the f wave of the final proton that has very small overlap with the s wave of

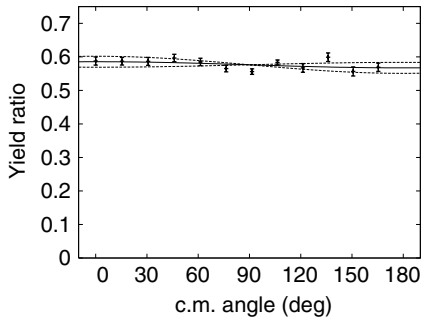

FIG. 6. Quotient of the proton yield divided by the α-particle yield. The angular distribution of the quotient is simulated by $a(1 + 2P_\sigma \cos\theta)$. The solid curve is for $P_\sigma = 0.008$ and $a = 0.576$. The dashed curves represent the range of $P_\sigma = 0.008 \pm 0.014$.

the deuteron, the main component of the incident wave. The deuteron D state is implicitly included as the internal freedom of the deuteron. Because the central force produces the dominant contributions to the reaction, the vector amplitudes ($K = 1$) will be dominant over other amplitudes. The vector components of the amplitudes due to the LS and tensor interactions are also included in this amplitude. Thus, as the first step, we neglected $F(s_i s_f K l_i)$, except for $K = 1$, and assumed $l_i = l_i' = 0$, which corresponds to the s-wave incident. Due to these approximations, we derived from Eqs. (9)–(11) the vector and tensor analyzing powers as

$$iT_{11} = 0, \tag{17}$$

$$T_{2q} = -\frac{2\sqrt{3}}{\sqrt{5}}\alpha_1 P_{2q}(\cos\theta), \tag{18}$$

$$\alpha_1 = \frac{X_{00}(1,1)}{Z_{00}(1,1)}, \tag{19}$$

where P_{kq} is the associated Legendre function and the magnitudes of T_{2q} for $q = 0, 1, 2$ are given by α_1, which can be treated as a flexible parameter. Later, α_1 is determined by including corrections due to the $K' = 2$ amplitudes and p and d waves. Figure 7 shows the calculation with the parameters in Table IV compared with the experimental data, where the $K = 1$ contribution by Eq. (18), which is described by the dashed lines, is found to reproduce the essential features of the measured T_{2q}. Then, before discussing the final result of the calculation, we examine the constituents of $X_{00}(11)$ and $Z_{00}(11)$ in Eq. (19) to see the role of each spin state specified by the channel spins, in the analyzing powers.

From Eqs. (14) and (16),

$$\begin{aligned} X_{00}(1,1) = {} & \frac{1}{4\sqrt{3}}|F(11)|^2 - \frac{1}{20\sqrt{3}}|F(12)|^2 \\ & + \frac{7}{20\sqrt{3}}|F(21)|^2 - \frac{7}{20\sqrt{3}}|F(22)|^2 \\ & + \mathrm{Re}\left\{\frac{2}{\sqrt{15}}F^*(01)F(21)\right. \\ & \left. - \frac{3}{2\sqrt{5}}F^*(11)F(21) + \frac{3}{10}F^*(12)F(22)\right\}, \end{aligned} \tag{20}$$

TABLE IV. Quantities $\alpha_1 \sim \alpha_5$, which were determined so as to fit the ^{6}Li(d, p_0) data, by a most-likelihood method.

P_σ	-0.006	0.008	0.022
α_1	-0.168 ± 0.027	-0.168 ± 0.027	-0.168 ± 0.027
α_2	0.043 ± 0.040	0.040 ± 0.040	0.036 ± 0.040
α_3	-0.006 ± 0.014	-0.008 ± 0.013	-0.010 ± 0.013
α_4	0.019 ± 0.027	0.019 ± 0.027	0.019 ± 0.027
α_5	0.006 ± 0.030	0.005 ± 0.030	0.005 ± 0.030

$$\begin{aligned} Z_{00}(1,1) = {} & |F(01)|^2 + |F(02)|^2 + |F(11)|^2 \\ & + |F(12)|^2 + |F(21)|^2 + |F(22)|^2, \end{aligned} \tag{21}$$

where $F(s_i s_f K l_i)$ is abbreviated as $F(s_i s_f)$ because K and l_i were fixed as $K = 1$ and $l_i = 0$. First, we show that one can extract information about the spin of the resonance state from the analyzing power data, assuming that the resonance state is specified by a particular spin and parity which produces dominant contributions to observables for instance the analyzing powers. Accordingly, amplitudes of configurations of other spin and/or parity are classified as the nonresonance component and are tentatively neglected. Among $s_i = 0, 1, 2$, it is sufficient to consider $s_i = 1$ and 2 for the resonance spin, because $s_i = 0$ appears only as an interference term in Eq. (20), and cannot contribute to T_{2q} when the partner amplitude vanishes. That is the amplitude of $s_i = 0$ does not dominate over other amplitudes in producing the analyzing powers. Thus one can exclude $s_i = 0$ from the candidate of the spin of the resonance, although the $s_i = 0$ amplitudes contribute to the cross section as seen in Eq. (21), $Z_{00}(1, 1)$ is proportional to the cross section. When $s_i = 1$ dominates (the parity is positive because of $l_i = 0$),

$$\alpha_1 = -\frac{p - 5}{20\sqrt{3}(1 + p)}, \quad p \equiv \frac{|F(12)|^2}{|F(11)|^2}. \tag{22}$$

The possible α_1 is in the range $-0.02887 \leqslant \alpha_1 < 0.1443$ due to $0 \leqslant p < \infty$. Then, α_1, which describes the measured tensor-analyzing powers, $\alpha_1 = -0.167 \pm 0.018$ (Table IV), deviates far from this range of α_1 and one cannot choose α_1 so as to reproduce the experimental data when $s_i = 1$. That is, $s_i = 1$ cannot explain the measured analyzing powers and then the spin and parity of the resonance cannot be 1^+. Contrary to that, when $s_i = 2$ dominates,

$$\alpha_1 = -\frac{7(1 - p)}{20\sqrt{3}(1 + p)}, \quad p \equiv \frac{|F(21)|^2}{|F(22)|^2}. \tag{23}$$

The range of possible α_1 is $-0.2021 \leqslant \alpha_1 < 0.2021$ because of $0 \leqslant p < \infty$. This range of α_1 includes $\alpha_1 = -0.167 \pm 0.018$. That means, in the case of $s_i = 2$, one can choose α_1 so as to fit the data. From these considerations, we could identify the spin and parity of the resonance state as 2^+. This assignment agrees with the conventional one for the spin-parity of the resonance and this agreement will support the basic idea of the present analysis. In the case of $s_i = 2$, $p = 0.095 \pm 0.053$. This indicates that spin-flip amplitudes ($s_f \neq s_i$) are considerably small compared with spin-nonflip amplitudes ($s_f = s_i$).

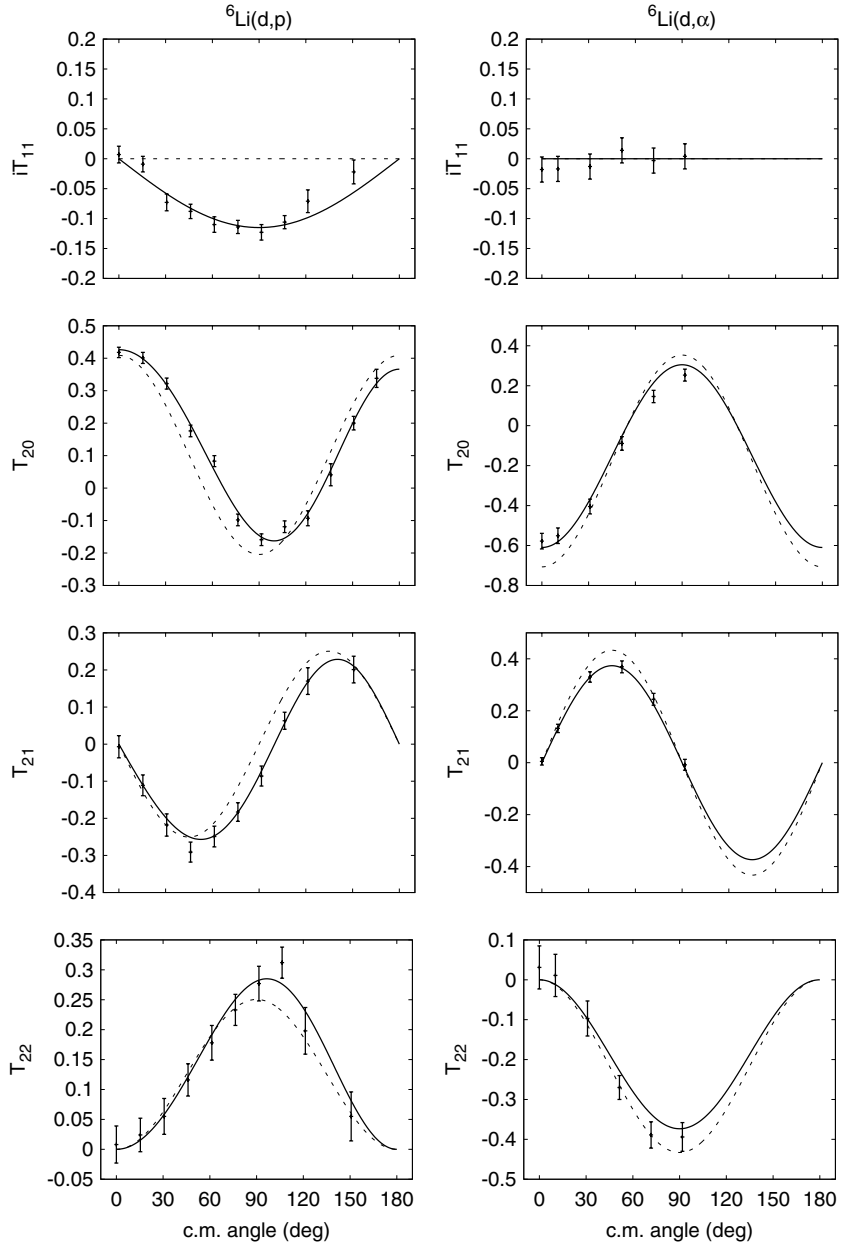

FIG. 7. (Left:) Experimental result for ^{6}Li$(d, p)^7$Li. The dashed curves represent the prediction by Eqs. (17)–(18) with $\alpha_1 = -0.167$. The solid curves represent the prediction by Eqs. (27)–(29) and (35) with parameters in Table IV and $\beta = -0.115$. (Right) Experimental results for ^{6}Li$(d, \alpha)^4$He. The dashed curves represent the prediction by Eq. (43). The solid curves represent the prediction by Eq. (45) with $f = 0.86$. The abscissas represent the scattering angle in the c.m. system.

Further, when the spin-flip amplitudes are neglected, we could estimate the fraction of the 2^+ component. We define the fraction by

$$f_R \equiv \frac{|F(22)|^2}{|F(11)|^2 + |F(22)|^2}. \tag{24}$$

From Eqs. (20) and (21),

$$\alpha_1 = \frac{5 - 12 f_R}{20\sqrt{3}}. \tag{25}$$

Using $\alpha_1 = -0.167 \pm 0.018$, we obtained

$$f_R = \frac{5 - 20\sqrt{3}\alpha_1}{12} \simeq 0.899 \pm 0.052. \tag{26}$$

In the second step, we refined the calculation by including contributions of the interference terms between $K = 1$ and 2, where the p and d waves in the incident partial wave are considered as long as they interfere with the s wave. Using Table V of Ref. [3], one can write the tensor-analyzing powers as follows:

$$T_{20} = \frac{1}{1 + 2P_\sigma \cos\theta}\left[-\frac{2\sqrt{3}}{\sqrt{5}}\alpha_1 P_{20} + \sqrt{15}\alpha_2 \cos\theta \sin^2\theta - 2\sqrt{6}\alpha_3 \cos\theta + \sqrt{15}\alpha_4 \sin^2\theta - \sqrt{6}\alpha_5\right], \tag{27}$$

$$T_{21} = \frac{1}{1 + 2P_\sigma \cos\theta}\left[-\frac{2\sqrt{3}}{\sqrt{5}}\alpha_1 P_{21} + \sqrt{\frac{5}{2}}\alpha_2(2\cos^2\theta - 1) \times \sin\theta + 3\alpha_3 \sin\theta + \sqrt{\frac{5}{2}}\alpha_4 \cos\theta \sin\theta\right], \tag{28}$$

$$T_{22} = \frac{1}{1+2P_\sigma \cos\theta}\left[-\frac{2\sqrt{3}}{\sqrt{5}}\alpha_1 P_{22} - \sqrt{\frac{5}{2}}\alpha_2 \cos\theta \sin^2\theta + \sqrt{\frac{5}{2}}\alpha_4 \sin^2\theta\right], \quad (29)$$

with

$$\alpha_2 = \frac{X_{01}(1,2)}{Z_{00}(1,1)}, \quad \alpha_3 = \frac{X_{01}(1,1)}{Z_{00}(1,1)},$$
$$\alpha_4 = \frac{X_{02}(1,2)}{Z_{00}(1,1)}, \quad \alpha_5 = \frac{X_{11}(1,1)}{Z_{00}(1,1)}, \quad (30)$$
$$P_\sigma = \frac{Z_{01}(1,1)}{Z_{00}(1,1)},$$

where α_3 and α_5 describe the p-wave corrections for the $K = 1$ amplitudes, and α_2 and α_4 describe the p- and d-wave contributions in the interference terms between amplitudes $K = 1$ and 2. As described in Sec. II, the angular distribution of the differential cross section was experimentally examined to obtain the information of P_σ. The measured cross section is shown in Fig. 6. The vertical axis represents the quotient of the cross section of ^{6}Li(d, p) divided by that of ^{6}Li(d, α). The quotient can be canceled by each solid-angle of the detectors. Because the cross section of ^{6}Li(d, α) is practically isotropic as discussed in Sec. III B, the anisotropy of the quotient is identical to that of ^{6}Li(d, p) cross section, which is considered to be p-wave effects. Finally, using Table I of Ref. [3], the cross section for ^{6}Li(d, p) is represented as

$$\sigma_p(\theta)/\sigma_\alpha(\theta) = a(1 + 2P_\sigma \cos\theta). \quad (31)$$

The quantities, a and P_σ are treated as flexible parameters and are determined so as to fit the experimental data in Table III by a most-likelihood method. The obtained parameters are $P_\sigma = 0.008 \pm 0.014$ and $a = 0.576 \pm 0.011$. Fixing the parameter P_σ in this range, the quantities $\alpha_1, \alpha_2, \ldots, \alpha_5$ are also treated as flexible parameters and are determined so as to fit the experimental data of the analyzing powers by a most-likelihood method. In Table IV, we gave as typical cases three sets of the parameters $(\alpha_1, \alpha_2, \ldots, \alpha_5)$ and P_σ. The deduced parameters α_i are almost constant for $0.008 - 0.014 \leqslant P_\sigma \leqslant 0.008 + 0.014$. Thus the analyzing powers hardly depend on such details of the angular distribution of the cross section. The analyzing powers, T_{2q} calculated with these parameters, are shown by solid curves in Fig. 7. They show good agreements with the data. Here, the most important correction is given by α_2, which describes the p-wave correction. It is noted that the magnitude of α_1 is not affected by including the anisotropy of the cross section. Because the contributions of the above corrections are small, we will neglect further corrections due to other terms, for example, those of $K = K' = 2$, which do not include the incident s wave.

To investigate the energy dependence of the theoretical parameter α's, the present analyses had been applied to the analyzing powers of higher-energy (d, p) reactions at 600 and 960 keV. For the convenience of comparison, their data [5], which are described in the Cartesian representation A_{ij}, were transformed to T_{2q} by the well-known relations [8]

$$A_{zz} = \sqrt{2}T_{20}, \quad (32)$$
$$A_{xz} = -\sqrt{3}T_{21}, \quad (33)$$
$$A_{xx} - A_{yy} = 2\sqrt{3}T_{22}. \quad (34)$$

Then T_{2q} derived have angular distributions similar to those at 90 keV. The calculation had successfully reproduced the analyzing-power data although they are not displayed in figures. In these cases, the magnitude of α_1 decreases, whereas other α's increase with the increase of the incident energy; for instance, α_1 obtained at 960 keV is reduced by about 20% compared to the one at 90 keV. This will mean that the 2^+ contribution that includes the resonance effects decreases with the increase of the energy and the non-resonance contributions such as the incident p wave one increase. For detailed analyses of such energy dependence, one will need more experimental data of the analyzing powers in this energy region.

A finite iT_{11} was obtained by including the p wave in the incident partial wave. By using Table IV of Ref. [3],

$$iT_{11} = \frac{1}{1+2P_\sigma \cos\theta}\beta \sin\theta \quad (35)$$

with

$$\beta = 3\beta_1 + \frac{3}{\sqrt{2}}\beta_2, \quad (36)$$

where β_1 describes the contribution of the $K = 1$ amplitude and β_2 that of the interference between the amplitudes $K = 1$ and 2,

$$\beta_1 = \frac{Y_{01}(1,1)}{Z_{00}(1,1)}, \quad \beta_2 = \frac{Y_{01}(1,2)}{Z_{00}(1,1)}. \quad (37)$$

In Fig. 7, iT_{11} calculated by Eq. (35) reproduced the data by fixing $\beta = -0.115 \pm 0.016$.

B. ^{6}Li(d, α)

Next, we analyzed the reaction ^{6}Li(d, α). In this case, $s_a = s_A = 1$ and $s_b = s_B = 0$. Thus, the initial channel spin is $s_i = 0, 1, 2$ and the final one is $s_f = 0$. The parity is not changed by the reaction $(\Delta P = 0)$. Thus, the transition by $K = 0(0^+ \to 0^+)$ and the one by $K = 2(2^+ \to 0^+)$ are allowed, and the transition by any central interaction from the 2^+ state is now forbidden. The $K = 0$ amplitude does not contribute to the tensor analyzing powers by itself and appears in T_{2q} only as an interference term with the $K = 2$ amplitude. Because the 2^+ configuration is the major amplitude and the 0^+ one is the minor one in the initial state, the $K = 2$ transition makes the main contribution and the $K = 0$ transition will give a correction. The total tensor-analyzing powers are given by

$$T_{2q} = T_{2q}(2,2) + \Delta T_{2q}, \quad (38)$$

where $T_{2q}(2, 2)$ is the contribution of the $K = 2$ transition term and ΔT_{2q} is the interference term between $K = 0$ and 2.

Keeping only the $K = 2(2^+ \to 0^+)$ transition, the analyzing powers are described for the s-wave incident as

$$T_{2q}(2,2) = \frac{1}{N_R} X_{00}(2,2) Q_{2q00},$$
$$N_R = Z_{00}(2,2) Q_{0000}, \tag{39}$$

where

$$Z_{00}(2,2) = |F(2020)|^2, \tag{40}$$

$$X_{00}(2,2) = \frac{\sqrt{7}}{10} |F(2020)|^2. \tag{41}$$

From Tables I and III in Ref. [3],

$$Q_{0000} = 1, \quad Q_{2q00} = -\frac{2\sqrt{5}}{\sqrt{7}} P_{2q} \tag{42}$$

From Eqs. (39)–(42), the $K = 2$ transition term is described as

$$T_{2q}(2,2) = -\frac{1}{\sqrt{5}} P_{2q}, \tag{43}$$

which is independent of the theoretical parameters.

From Eq. (2.13) in Ref [3], the interference term is described as

$$\Delta T_{2q} = \frac{\mathrm{Re}\{F^*(0000)F(2020)\}}{|F(2020)|^2 + |F(0000)|^2} \cdot \frac{2\sqrt{2}}{\sqrt{5}} P_{2q}. \tag{44}$$

Totally,

$$T_{2q} = -\frac{1}{\sqrt{5}} f P_{2q}, \tag{45}$$

where

$$f = \left(1 - 2\sqrt{2}\frac{\mathrm{Re}\{F^*(0000)F(2020)\}}{|F(2020)|^2}\right) f_R, \tag{46}$$

with

$$f_R = \frac{|F(2020)|^2}{|F(2020)|^2 + |F(0000)|^2}, \tag{47}$$

which describes the fraction of the 2^+ component. Figure 7 shows a comparison of the experimental data with the theoretical prediction. There, the $K = 2$ transition term Eq. (43), which is described by the dashed lines, explains most of the measured analyzing powers in both of the magnitudes and the angular distributions without any adjustable parameter. This means that the decay of the 2^+ state is the dominant mechanism of the transition. The total calculation by Eq. (45) with $f = 0.862 \pm 0.087$ is described by the solid lines and gives good agreements with the data, where the correction due to the $K = 0$ amplitude is clarified to be small. From Eq. (46), we derived the order of magnitude of the $K = 0$ amplitude in the first order in the following form

$$\frac{\mathrm{Re}\{F^*(0000)F(2020)\}}{|F(2020)|^2} = \frac{1-f}{2\sqrt{2}} = 0.0488, \tag{48}$$

which is very small compared to 1. More detailed estimation was made for f_R by using the approximation,

$$|\mathrm{Re}\{F^*(0000)F(2020)\}| \simeq |F(0000)||F(2020)|. \tag{49}$$

The approximation is valid when the imaginary parts of the amplitudes are small compared to the real ones and, at low energies, the real interactions are more important than the imaginary ones as the general trend. In the present case, the approximation provides a typical value of f_R for small $|F(0000)|/|F(2020)|$. Using above, we had f_R from Eq. (46) by taking the terms up to $n = 2$ in the expansion by $(1-f)^n$,

$$f_R \simeq \left[1 + \tfrac{1}{8}(1-f)^2\right]^{-1}. \tag{50}$$

Substituting the experimental value ($f = 0.862 \pm 0.087$), we obtained the 2^+ fraction $f_R = 0.9976 \pm 0.0030$. Then the $s_i = 0$ configuration has a very small fraction and the contribution to T_{2q} is enhanced by the interference with the $s_i = 2$ configuration. Contributions of the incident d wave to T_{2q} have been examined by formulas similar to those for the p wave effect in the (d, p) reaction (see Appendix), where f and the d-wave parameter P_σ are treated as flexible parameters. To fit the analyzing-power data of the (d, α) reaction, we obtained $f = 0.877 \pm 0.087$ and $P_\sigma = -0.046 \pm 0.077$, where the magnitude of f agrees with the previous value within the experimental errors and P_σ is small compared to the errors and practically will be approximated by zero. Thus, at the present energy, one will neglect the anisotropy of the angular distribution of the (d, α) cross section due to the incident d wave. To examine the validity of this approximation, we calculated the differential cross section by Eq. (A5) at higher energies up to 975 keV. The calculation describes well the measured cross sections [13] within the experimental errors. The energy dependence of P_σ obtained is shown in Fig. 8, which suggests P_σ at $E_\mathrm{d} = 90$ keV to be very small in an extrapolation consideration.

To see the energy dependence of f, we extended the analysis of the $(d, \alpha)T_{2q}$ data to higher energies up to $E_d = 960$ keV, including the incident d-wave effect with P_σ obtained above which is simulated by a smooth function of the incident energy. The calculated analyzing powers reproduced the feature of the measured ones [14] although the quality of the agreement between the calculated and the measured becomes worse at higher energies, particularly for T_{22}. In Fig. 9, the obtained f is shown as the function of the incident energy, which decreases with the increase of the energy, remarkably

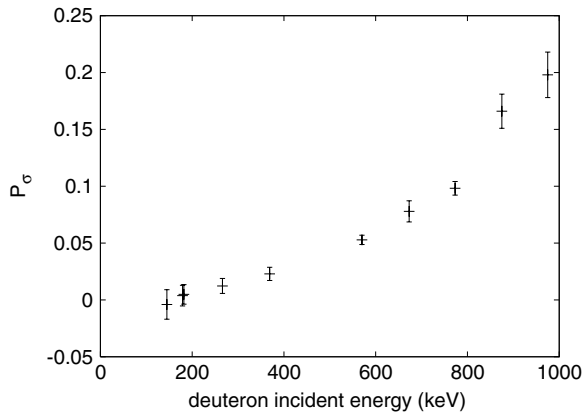

FIG. 8. Energy dependence of the theoretical parameter P_σ.

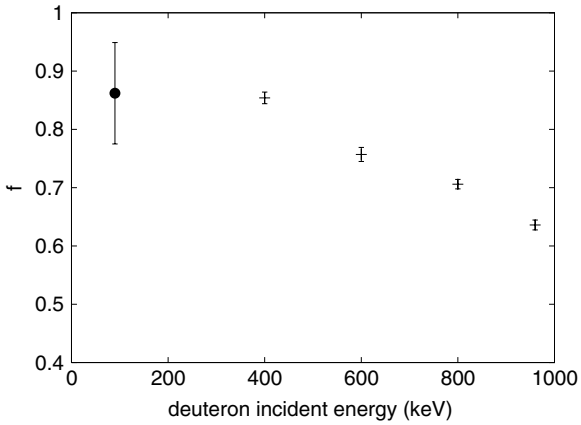

FIG. 9. Energy dependence of the theoretical parameter f.

beyond $E_d = 400$ keV. More detailed investigations of the analyzing powers at such energies will be useful to obtain information about the nature of the 2^+ resonance [12].

The vector-analyzing power, iT_{11}, is zero because the invariant amplitude includes the factor $1 + (-)^{l_f}$ and $l_f = 1$ for iT_{11} when the residual and the ejectile particles are identical. The data of the analyzing power is consistent with the prediction, as can be seen in Fig. 7.

IV. SUMMARY AND DISCUSSION

We measured the vector- and tensor-analyzing powers of the polarized deuteron for the ^{6}Li$(d, p_0)^7$Li and ^{6}Li$(d, \alpha)^4$He reactions at the very low incident energy, 90 keV. We analyzed the data by the invariant amplitude method in a model-independent way and found that the 2^+ configuration with the d-^{6}Li s-wave provides the dominant contributions to the tensor analyzing powers in both reactions. In the (d, p) reaction, the nonresonance 1^+ configuration of the $d + ^6$Li system contributes to the tensor-analyzing powers by order of magnitude 10% of the measured. Other corrections due to the non resonance component had been taken into account by including the p- and d waves in the incident channel for the (d, p_0) reaction. For the (d, α) reaction, the 0^+ state of the $d + ^6$Li system was taken into account as the correction. The calculations, which included these corrections, gave excellent agreement with the data. The measured vector-analyzing power in the (d, p_0) reaction had been explained as an interference effect between the incident s and p waves, and that in the (d, α) reaction was almost zero, which is consistent with the 2^+ resonance assumption.

The fractions of the 2^+ configuration, which includes the resonances, in the reactions were estimated from the analyzing power data; the fraction in the (d, p_0) reaction was 0.899 ± 0.052, which is comparable to that of the resonance derived by the analysis of the cross section; also, the 2^+ fraction in the (d, α) reaction was 0.998 ± 0.003, which is much larger than the fraction of the resonance estimated from the S factor by the use of the cross section, which was analyzed by a compound-nucleus plus DWBA model [2]. The analyzing power data for both of (d, p) and (d, α) reactions at higher energies up to 960 keV were analyzed by the present method, which provided information of the energy dependence of the 2^+ state fraction. These results will be valuable in the field of nuclear astrophysics and thereby analyses of the analyzing powers, such as the present one, will be one favorable approach, because the analyzing powers can be measured with some desirable accuracies even at low incident energies. Thus, we hope to realize extensive applications of the analyzing-power method in the future.

Finally, it should be noted that examinations will be worthwhile if the measured analyzing powers are explained by adopting particular reaction models, because such approaches will provide a comprehensive understanding of the nature of the reaction. For example we will examine the analyzing powers for the (d, α) reaction by the compound-nucleus plus DWBA model employed in the cross-section analysis in Ref. [2]. The compound-nucleus amplitude does not provide the analyzing powers due to lack of spin-dependent interactions as seen in Eq. (8). For the DWBA part, we had calculated the analyzing powers by the zero-range DWBA used in Ref. [2], but including a deuteron LS interaction that was neglected in Ref. [2]. However, at present, we have not yet obtained successful results, although many parameter sets of the optical potentials have been examined.

ACKNOWLEDGMENTS

The authors deeply thank the staff of UTTAC for maintaining the good experimental circumstance.

APPENDIX: EXPRESSIONS OF CROSS SECTION AND ANALYZING POWERS OF THE (d, α) REACTION WHEN THE INCIDENT d WAVE IS CONSIDERED

Equation (45) for the tensor-analyzing powers of the (d, α) reaction are modified by the inclusion of the interference terms between the incident s wave and d wave. Using $Q_{2q02}(2, 2)$ in Table III in Ref. [3],

$$T_{2q} = \frac{1}{1 + P_\sigma(3\cos^2\theta - 1)}\left(\frac{-1}{\sqrt{5}} f P_{2q} + \Delta_{2q}\right) \quad \text{(A1)}$$

$$\Delta_{20} = -\frac{1}{\sqrt{2}} P_\sigma(3\cos^2\theta - 1) \quad \text{(A2)}$$

$$\Delta_{21} = \frac{\sqrt{3}}{2} P_\sigma \cos\theta \sin\theta \quad \text{(A3)}$$

$$\Delta_{22} = \frac{\sqrt{3}}{2} P_\sigma \sin^2\theta \quad \text{(A4)}$$

and the cross section $\sigma_\alpha(\theta)$ is given by

$$\sigma_\alpha(\theta) = \sigma_0[1 + P_\sigma(3\cos^2\theta - 1)], \quad \text{(A5)}$$

where σ_0 is a constant and P_σ is defined as

$$P_\sigma = \frac{\mathrm{Re}\{F^*(2020)F(2022)\}}{|F(2020)|^2 + |F(0000)|^2}. \quad \text{(A6)}$$

[1] J. E. Monahan, A. J. Elwyn, and F. J. D. Serduke, Nucl. Phys. **A269**, 61 (1976).
[2] K. Czerski, A. Huke, H. Bucka, P. Heide, G. Ruprecht, and B. Unrau, Phys. Rev. C **55**, 1517 (1997).
[3] M. Tanifuji and H. Kameyama, Phys. Rev. C **60**, 034607 (1999).
[4] K. Czerski, H. Bucka, P. Heide, and T. Makubire, Phys. Lett. **B307**, 20 (1993).
[5] M. Glor, H. P. Naegele, G. Morgan, R. Neff, H. Rudin, and F. Seiler, Nucl. Phys. **A286**, 31 (1977).
[6] Y. Tagishi and J. Sanada, Nucl. Instrum. Methods **164**, 411 (1979).
[7] G. G. Ohlsen, J. L. McKibben, G. P. Lawrence, P. W. Keaton Jr., and D. D. Armstrong, Phys. Rev. Lett. **27**, 599 (1971).
[8] G. G. Ohlsen, Rep. Prog. Phys. **35**, 717 (1972).
[9] M. Tanifuji, Phys. Lett. **B289**, 233 (1992).
[10] F. Ajzenberg-Selove, Nucl. Phys. **A490**, 1 (1988).
[11] D. R. Tilley, J. H. Kelley, J. L. Godwin, D. J. Millener, J. E. Purcell, C. G. Sheu, and H. R. Weller, Nucl. Phys. **A745**, 155 (2004).
[12] P. R. Page, Phys. Rev. C **72**, 054312 (2005).
[13] A. J. Elwyn, R. E. Holland, C. N. Davids, L. Meyer-Schutzmeister, J. E. Monahan, F. P. Mooring, and W. Ray Jr., Phys. Rev. C **16**, 1744 (1977).
[14] R. Neff, P. Huber, H. P. Nägele, H. Rudin, and F. Seiler, Helv. Phys. Acta **44**, 679 (1971).